Laser Cutting Coupled with Electro-Exfoliation to Prepare Versatile Planar Graphene Electrodes for Energy Storage

Jianren Wang, Tianshuo Yang, Neus Vilà, Alain Walcarius

International Journal of *Molecular Sciences*

MDPI

Article

Laser Cutting Coupled with Electro-exfoliation to Prepare Versatile Planar Graphene Electrodes for Energy Storage

Jianren Wang [1,2], Tianshuo Yang [2] , Neus Vilà [1] and Alain Walcarius [1,*]

[1] Université de Lorraine, CNRS, Laboratoire de Chimie Physique et Microbiologie pour les Matériaux et l'Environnement (LCPME), F-54000 Nancy, France; alain.walcarius@univ-lorraine.fr
2 Key Laboratory of Applied Chemistry, School of Environmental and Chemical Engineering, Yanshan University, Qinhuangdao 066004, Hebei, China; wangjr@ysu.edu.cn
* Correspondence: alain.walcarius@univ-lorraine.fr; Tel.: +33 3 72 74 73 75

Abstract: The study of planar energy storage devices characterized by low-cost, high capacity, and satisfactory flexibility, is becoming a valuable research hotspot. Graphene, monolayer sp^2 hybrid carbon atoms with a large surface area, always act as its active component yet with a tension between high conductivity and easy to implement. Although the difficult-to-assemble graphene can easily achieve planar assemblies in its highly oxidized form (GO), the undesired conductivity, even after proper reduction, still restricts its further applications. Here, a facile "Top-down" method has been proposed to prepare the graphene planar electrode via in-situ electro-exfoliation of graphite supported on a piece of laser-cutting patterned scotch tape. Detailed characterizations have been performed to study its physiochemical property evolution during electro-exfoliation. The obtained flexible graphene planar electrodes show a decent energy storage performance, e.g., 40.8 mF cm^{-2} at a current density of 0.5 mA cm^{-2} and a 81% capacity retention at a current density of 8 mA cm^{-2} for the optimized sample G-240. Their high conductivity also makes them possible to couple with other redox-active materials by electrodeposition to improve their performance, e.g., ferrocene-functionalized mesoporous silica film (Fc-MS), MnO_2, and polyaniline (PANI). The highest capacity is achieved with the PANI functionalized sample, which achieves a 22 times capacity increased. In a word, the versatility, practicality, and adaptability of the protocol to prepare the planar graphene electrode proposed in this work make it a potential candidate to meet the continuously growing energy storage demands.

Keywords: pseudocapacitive materials; graphene; planar electrode.

Citation: To be added by editorial staff during production.

Academic Editor: Firstname Lastname

Received: date
Revised: date
Accepted: date
Published: date

1. Introduction

The last few decades have witnessed the continuously surging demands of flexible and wearable microelectronics in various fields, such as biomedical sensors, wearable products, and sports assist devices, etc [1,2]. Therefore, beyond higher energy and power densities, these cutting-edge applications put forward more rigorous requirements for energy storage systems, including ease of miniaturization, robust mechanical properties, as well as high flexibility [3]. Generally, conventional energy storage devices, mostly composed of vertical sandwich structures with two electrodes, one separator membrane, and filled with liquid electrolyte, are too difficult to be fabricated into flexible micro-devices due to the complexity of such configuration [4]. In contrast, in-plane interdigitated devices, comprising flatly aligned but spatially separated energy storage materials with electrolyte coating onside directly, have gained more and more research interest in recent years. This idiosyncratic design offers several merits over the traditional sandwich structure in terms of the emerging application scenarios, such as:

- the distance between the adjacent working and coun-

ter electrodes could be minimized to some extent through advanced patterning techniques, which could reduce the internal resistance of the devices and improve their power output [5];

- the monolayer nature of the in-plane structure could largely increase the volume energy density by decreasing the thickness of devices, and also reduce short-circuit risks triggered by the external forces;
- the simplified architecture also makes it easier to be incorporated into electronic devices, and even suitable as the wearable power source when utilizing superior flexible supporting materials as substrates that can bear the long-term twisting and folding distortions.

Featured with a large surface area (~2630 m^2 g^{-1}), excellent electrical conductivity (~104 S cm^{-1}), and robust mechanical properties (Young's modulus of ~1TP) [6], graphene is widely used as the active material for flexible in-plane energy storage devices when integrated on various flexible substrates, such as polyethylene terephthalate (PET), polydimethylsiloxane (PDMS), and textiles, for instance [7–9]. Instead of directly utilizing graphene, graphene oxide is mostly used as the starting material to assemble these devices owing to its abundant functional groups, hydrophilic property, and high surface adhesion energy [10]. However, after the reduction processes, the products, so-called reduced graphene oxide, cannot recover the pristine graphene structure either in thermal, chemical, or electrochemical ways; therefore they always suffer from relatively low conductivities [11]. Besides, one more technical difficulty to fabricate such devices lies in precisely patterning graphene on substrates to make full use of the surface space while avoiding the short-circuit problem. Several possible strategies have been developed in recent years, including chemically coating graphene on pre-patterned current collectors [12], laser writing on in-situ reducing graphene oxide [13], plasma etching [14], and inkjet printing [15]. Nevertheless, these methods are still facing some drawbacks: dependence on sophisticated facilities, complicated preparation processes, utilization of organic solvent, and limited graphene-loading amount. As such, developing a low-cost and facile method to assemble high-quality graphene on flexible substrates in a dense and patterned way is pivotal to promoting the development of this kind of device.

Electro-exfoliation is an efficient protocol to produce various types of two dimensional materials from their bulk counterparts in a scalable fashion [16]. This method can also be used to exfoliate bulk graphite into mono/few layers through a coupling of electric filed driven sulfate ions intercalation and anodic water oxidation processes [17]. The flakes produced with such a method always show a high C/O ratio (~20) over other "Top-down" chemical methods (e.g., ~2 of Hummers method) [18], indicative of a small number of defects; as reported previously only the edge of the flakes can be oxidized [19]. Therefore, their properties, particularly electrical conductivity, should be more similar to graphene than graphene oxide [19], making them good candidates for energy storage electrodes. However, the as-formed graphene flakes are more likely to be peeled into the solution phase due to the intense bubbles produced by the constant water decomposition and the lack of binding sites at the graphite electrode. Although an "in-situ exfoliate and deposit" method has been developed to assemble vertically aligned graphene on conductive substrate [20], the graphene density of the final electrode is still relatively low, leading to a limited areal capacitance. If one tears a piece of graphite film with scotch tape to form a composite, the sticky tape surface would prevent the flakes from stripping during the electro-exfoliation process, and finally creates a scotch tape confined densely packed graphene electrode, and this is what we plan to investigate in the present work. Besides, the underlying scotch substrate also has several advantages, as discussed hereafter. The inherent characteristics of the scotch tape permit this electrode a high flexibility and robust mechanical nature, which makes them suitable for increasingly complex application scenarios. The pattern of the scotch tape can even be finely edited with a laser-cutting technique, which could be a low-cost, time saving, and versatile way to fabricate the in-plane planar devices. More than the substrate, the high conductivity and

large surface area of the graphene layer also make it easy to further composite with other energy storage active materials. As a proof of concept, we will evaluate here some modifiers that can be easily electrodeposited, such as, manganese dioxide (MnO_2), polyaniline (PANI), and redox molecules (i.e., ferrocene moieties) functionalized mesoporous silica films. Overall, a complete protocol to fabricate the planar graphene and/or its composite energy storage electrodes is proposed here, and the obtained electrodes not only show decent energy storage abilities but also permit adequate mechanical properties, which may have the opportunity to be used in the next-generation flatly flexible energy storage devices.

2. Results and discussions

2.1. Preparation of the planar graphite electrodes

The electrode preparation process is illustrated in Figure 1a, and as one can see, the laser first easily engraves the scotch tape to obtain different designed patterns, which can be further used to peel off a piece of graphite film from a graphite foil via its sticky surface. The resolution of this technique can reach here 800 μm, which suits the miniaturization of the next-generation energy storage devices. Please also note that there is still a room for optimization, and higher resolution might be achieved with the advanced laser generator.

This graphite-scotch tape composite undergoes a following electro-exfoliation process to fabricate the final flatly flexible graphene electrodes. Figure 1b gives the current profile of the electro-exfoliation process along with the corresponding digital photos of the electrode at a certain time. One can see that after a fast drop from 75 mA cm^{-2} to 60 mA cm^{-2} within a few seconds, the exfoliation current gradually goes down from 60 mA cm^{-2} to 10 mA cm^{-2} until the exfoliation time reaches ca. 250 s, and then faces a steady region after that. The initial sharp fall of the current is probably due to the formation of an electrical double-layer process, which could normally finish the charging within a few seconds. Afterward, the anodic current mainly comes from the sulfate ions inserted into the graphite interlayers and the oxygen evolution reaction [21], both of which help to expand and separate the graphite layer into mono/few layers of graphene. The continuously decreased current indicates the consumption of the graphite reactant and the increasing resistance of the graphite/scotch electrode because the inserted sulfate ions inside the exfoliated graphene could deteriorate the conductivity, as confirmed by the later activation experiments. The following current-steady region could be a signal that all graphite on scotch tape has been converted into graphene. The residue current could be a balance of the inserted sulfate ions between the electrical driving force and the thermodynamic distribution. Different from the almost constant current of directly electro-exfoliating graphite foil (Figure S1a), the gradually decreased current and the almost clear final solution (Figure S1b) indicate the scotch tape confinement effect towards its onside graphite, and the following characterizations will also prove that. The digital photos of the electrode with distinct exfoliation time show the color of the exfoliated material, the part above the yellow line gets darker with prolonging the exfoliation, indicating a structural change.

Taking the 240 s exfoliation sample (G-240) as an example, the conductivity change has been studied by both the AC impedance (Figure 1c) and the DC I-V curve (Figure 1d) to prove the need of the activation process at the potential of 0V (v.s. Ag/AgCl, 3 M). From the Nyquist plot of the impedance spectra, two kinds of shape can be observed, and obvious semicircle can be observed for the G-240 before activation sample, which may come from the charge transfer between graphite and the intercalated sulfate ions. Therefore, two equivalent circuits have been used to fit them. An extra R_{ct} element in parallel to the constant phase element (CPE) has been added in the equivalent circuit for graphite and G-240 sample. There corresponding circuits and detailed fitting results are given in Table S1. As can be seen, the resistance of the graphite/scotch electrode is ~0.7

Ω, while its resistance surges to as high as 1,145 Ω after the electro-exfoliation process, which might be due to deterioration from the intercalated sulfate ions. Fortunately, the intercalated sulfate ions can be reversibly repelled out to solution by applying a 0V potential onside for another 240 s, and the current of this activation process is shown in Figure S2. A strong cathodic current density ranging from -35 mA cm^{-2} to -1 mA cm^{-2} can be first observed at the beginning of 40 s, which may come from the fast move-out of the negatively charged sulfate ions located at the surface/near-surface of graphene. For the period from the 40 s to 240 s, the current delivers a slowly decreased trend from -1 mA cm^{-2} to -0.25 mA cm^{-2}, and the much smaller but relatively steady current may reflect the leaching of sulfate ions from the lattice of few layers of graphene and un-exfoliated graphite. After the activation, most sulfate ions are removed from the graphene electrode, and the conductivity of G-240 recovers back to 2.21 Ω. The similar resistance change of this process can also be confirmed by the DC I-V test, where two platinum clamps with 0.5 cm in width well contact the targeted sample in a distance of 2 cm. The resistances of graphite electrode, G-240, and G-240 before activation are respective 3.1 Ω, 8.1 Ω, and 20,740.8 Ω in our test condition.

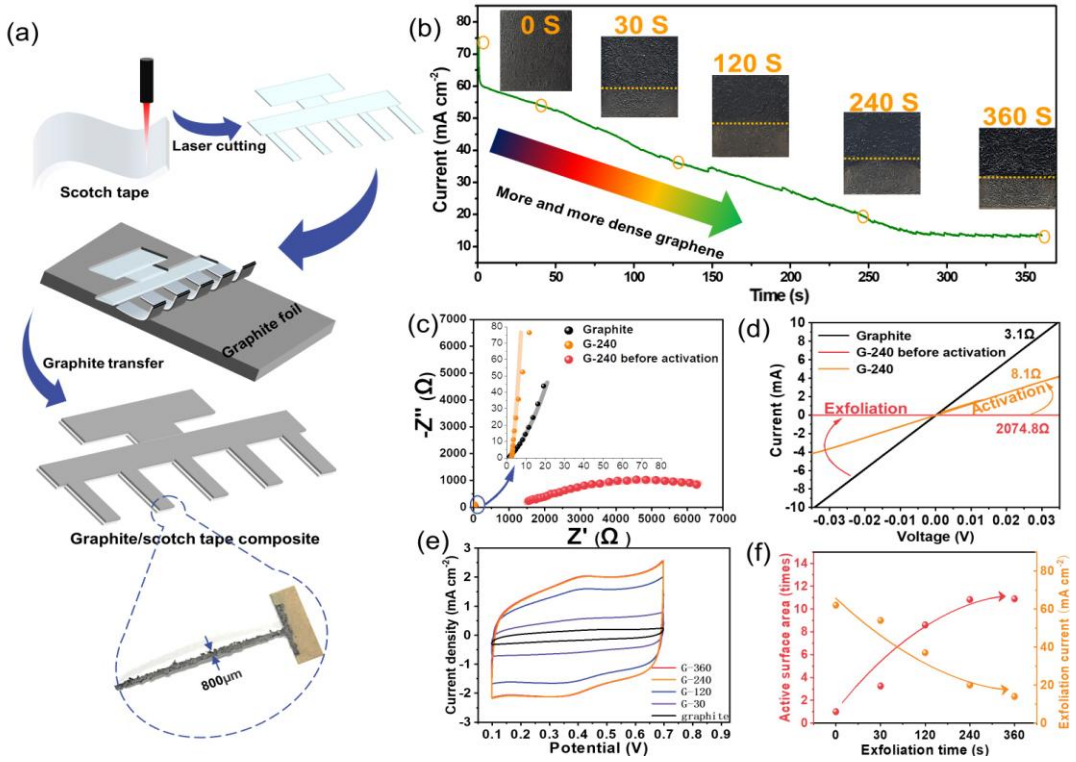

Figure 1. The preparation processes and some features of the planar graphene electrodes. (**a**) The illustration of the preparation process with an editable pattern; (**b**) the current measured during the preparation process (current density variation with time of exfoliation), and corresponding digital photos of the electrodes at a certain exfoliation times; (**c**,**d**) the impedance spectra (**c**) and the I-V curves (**d**) of the graphite electrode and the graphene electrode with 240s exfoliation time respectively before and after activation; (**e**) the CV curves of the graphene electrodes prepared with different exfoliation times at 50 mV s^{-1} in 1M H_2SO_4 electrolyte (*vs.* Ag/AgCl 3 M); (**f**) the electroactive surface area and the exfoliation current for different exfoliation times obtained from (**b**) and (**e**), respectively.

Besides, the relation between the exfoliation time and the electroactive area has also been analyzed by the cyclic voltammetry (CV) method. (Figure 1e) With prolonging the exfoliation time, the corresponding sample shows the current response steadily increases to 11 times until 240 s, and then reaches a stable state afterward. (Please note the active area here is not the actual area of the electrode but only reflects the increased times of the area) While the exfoliation current gives an opposite trend, it decreases first and then almost stays stable. This phenomenon not only proves the feasibility of using elec-

tro-exfoliation to prepare large surface area graphene electrodes but also demonstrates the exfoliation current could be used as an indicator to evaluate the density of graphene. The G-240 is therefore the optimized sample, and its related physiochemical properties as well as energy storage abilities are further evaluated in following.

2.2. Physico-chemical characterization of the planar graphite electrodes

The proposed graphene formation process during the electro-exfoliation is illustrated in Figure 2a. The intercalation of sulfate ions inside the interlayer of graphite would weaken the interaction between the adjacent graphene layers and the simultaneous oxygen gas evolution will tear them into graphene. The XRD patterns variation with different exfoliation time (Figure S3) prove this assumption to some extent, as the decreased intensity and the widening half-peak width of the (002) peak with extending the exfoliation time indicates the insertion of sulfate ions will affect the integrity of the graphite lattice. Besides, from our observation, long-time exfoliation will also lead to a stronger peak at ca.17o, which might be due to the formation of the sulfate intercalated graphite [22].

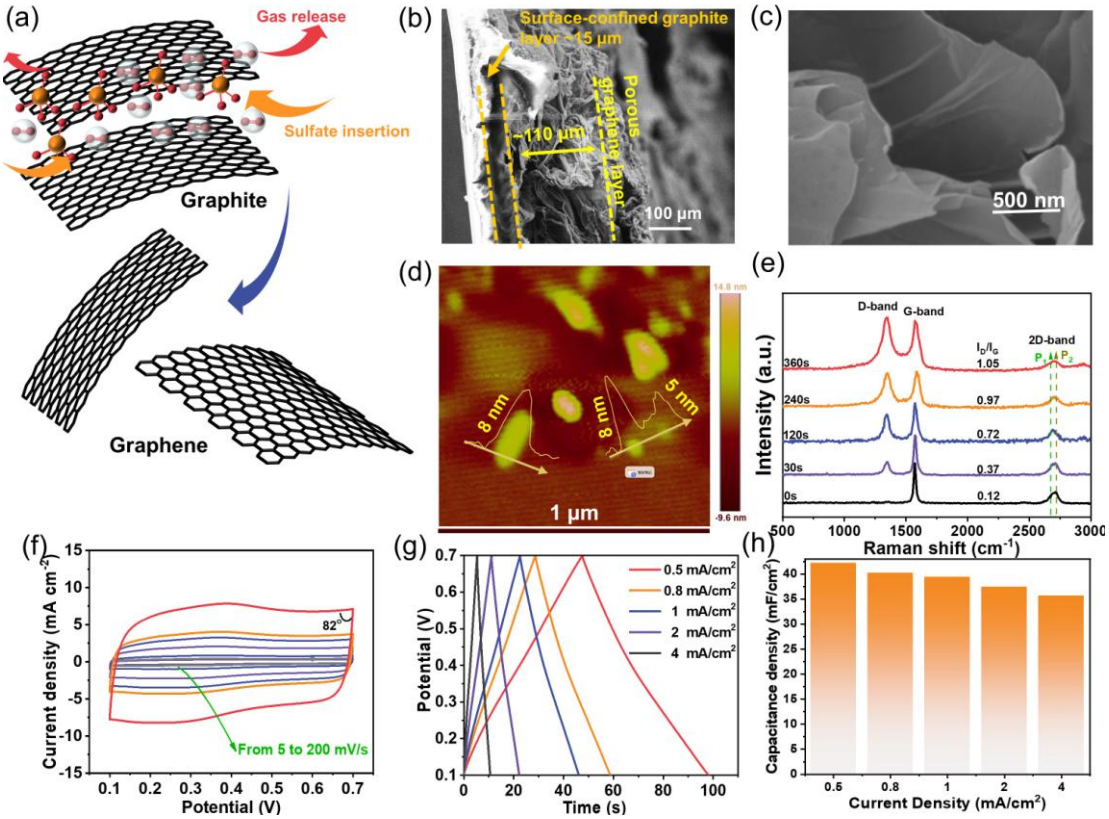

Figure 2. The detailed physiochemical properties of the prepared electrodes (especially G-240) and the energy storage abilities of G-240. (**a**) the illustration of the conversion from graphite to graphene during the electro-exfoliation process; (**b**,**c**) the respective cross-section (**b**) and high-resolution (**c**) SEM images of the G-240; (**d**) the AFM image of the fakes from G-240; (**e**) the Raman spectra of the sets of graphene electrodes; (**f**) the CV curves of G-240 from the scan rates of 5 to 200 mV s^{-1} in the solution of 1M H_2SO_4 (*vs.* Ag/AgCl 3 M); (**g**,**h**) the charge-discharge curves and corresponding capacitance of G-240 at the current densities from 0.5 to 8 mA cm^{-2}, respectively.

The microstructure of the graphite/scotch electrode and G-240 electrode have been characterized by scanning electron microscopy (SEM). The cross-section view of the original graphite/scotch tape electrode (Figure S4) shows a compact graphite layer with a thickness of ~50 μm, and the underlying brightest region that arose from the charge accumulation effect is the insulating scotch tape substrate. After the exfoliation, the cross-section of G-240 (Figure 2b) shows that the material becomes heterogeneous. It is

composed of two distinct layers: the highly porous top layer with the thickness swelling to ca.110 μm due to the oxygen bubbles impact, and the layer near the scotch tape with the thickness ca.15 μm, which seems not being affected by the exfoliation process and still manifests the pristine graphite structure due to the scotch-tape confinement effect. Further, the high-resolution SEM image (Figure 2c) of the top layer also reveals it is composed of few layers graphene, which is also confirmed by the AFM result (Figure 2d) with a thickness of 5~8 nm and the almost transparent flakes from the TEM image (Figure S5). The anisotropic structure feature of G-240 could benefit its energy storage application, notably because the highly porous graphene top layer will not only possess continuous channels for counter ions diffusion and but also provide large surface area for the energy storage or even compositing with other active materials. In addition, Raman spectra (Figure 2e) also demonstrate the electro-exfoliation will also alter the carbon hybridization status, as the ratio of D-band (sp3 hybridization)/G-band (sp2 hybridization) increases with extending the exfoliation time. The gradually increased D-band might arise from the surface oxidation of the carbon basal plane, and/or the edge sites of the newly formed graphene [23]. The 2D-band, sensitive to the layer of graphene, has also been observed for different samples. For monolayer graphene, its intensity should be much higher than that of G band. However, this is not the case for our samples, and similarly low intensities 2D bands have been observed for all samples. This can be ascribed to the composite nature of our samples, as the graphite layer next to the scotch tape cannot be exfoliated. Despite this, their noticeable shape change can be observed for different exfoliation time. The shoulder peak of graphite at the lower Raman shift (P_1) gradually increases with extending exfoliation time, indicative of the formation of few-layers graphene [24]. While the intensity of P_2 peak gradually decrease, suggesting the reduced ratio of graphite in the composites.

As mentioned above, the G-240 is the most "cost-effective" sample and therefore its energy storage properties have been evaluated in detail. The CV curves of G-240 are recorded at various scan rates from 5 mV s^{-1} to 200 mV s^{-1} in 1M H_2SO_4 aqueous solution. The corresponding results (Figure 2f) show a rectangular shape, despite a pair of very small redox peaks at ca. 0.35 V coming from oxygen-containing functional groups [25] (to clarify this pair of peaks, the CV curve at a low scan rate of 1 mV/s is given in Figure S6), no matter at the relatively low scan rate of 5 mV s^{-1} or at the high scan rate of 200 mV s^{-1}. This behavior is a double-layer type process, where the charges are accumulated on the surface of conductive surface, and the counter ions are physically adsorbed onside the surface of the electrode by the potential driven force at the meantime. There is no charge could transfer across the interface during the formation of the double-layer, and therefore its behavior can be described as a capacitor in the equivalent circuit. Besides, the well-maintained rectangular shape and the nearly 90° turning at the switching potential (even 82° at the scan rate of 200 mV s^{-1}) further demonstrate the negligible internal resistance and fast ions diffusion process during charge-discharge processes. The energy storage ability of G-240 is assessed with the galvanostatic charge-discharge technique (Figure 2g) with current densities from 0.5 mA cm^{-2} to 8 mA cm^{-2}. Despite a slight distortion at ca. 0.35 V, the symmetrically triangular charge-discharge curves show the pure electrical double-layer energy storage process and high coulombic efficiency. Based on these curves, the G-240 shows a high-rate performance with 40.8 mF cm^{-2} at a current density of 0.5 mA cm^{-2} (49 s charge/discharge time) and 81% (33.0 mF cm^{-2}) retention at a high current density of 8 mA cm^{-2} (2 s charge/discharge time). Unsurprisingly, the G-240 delivers a robust cycling performance (Figure S7). Besides, there is no obvious difference between the impedance of the original G-240 and that after its long-term cycling, which indicates its stable structure (Figure S8).

2.3. Modification of the planar graphite electrodes to get pseudocapacitive materials

Rather than using them alone, as aforementioned, the large surface area and good electrical conductivity of graphene electrodes make it possible to further turn them into

nanocomposites with associating other redox-active materials in order to improve their energy storage performance. Facile electrodeposition methods have been adopted for the modification of G-240, respectively with ferrocene functionalized mesoporous silica film (Fc-MS), manganese dioxide (MnO_2), and polyaniline (PANI), as illustrated in Figure 3a.

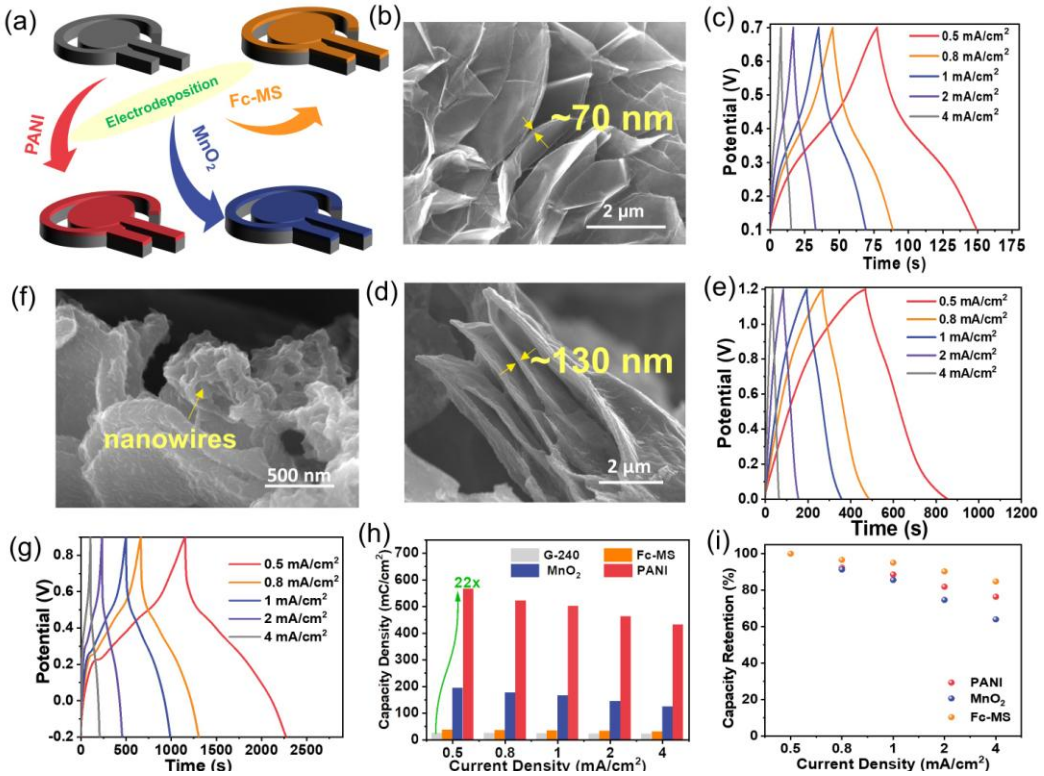

Figure 3. The preparation of the binary composites between G-240 and Fc-MS, MnO_2 or PANI by electrodeposition methods. (**a**) The illustration of the composition between graphene and corresponding redox active materials; (**b**-**g**) the typical SEM images (**b**,**d**,**f**) and energy storage abilities (**c**,**e**,**g**) of G-240 functionalized with Fc-MS, MnO_2 or PANI, respectively; (**h**,**i**) the calculated capacity density (**h**) and rate performance (**i**) of corresponding materials.

The corresponding SEM images (Figure 3b,3d, & 3f) and elements mapping results (Figure S9) reveal that all three redox-active components have been well integrated on the surface of graphene, yet in different forms. The Fc-MS and MnO_2 cover the graphene nanosheets in the film with a thickness of ~70 nm (similar to our previous report [26]) in the former case, and 130 nm in the latter case. In contrast, the electropolymerized PANI was found to independently grow on the graphene surface in a nanowires form. The loading mass of PANI and MnO_2 onside the G-240 are 1.9 mg/cm^2, and 3.1 mg/cm^2. Regarding the Fc-MS functionalized sample, the loading of the ferrocene molecules is in a trace amount, which is below the detection limit of the balance. But our previous work has proved that almost all ferrocene molecules are redox active [26]. Please note that not limited to the three components given here, these results demonstrate the prepared graphene electrode can act as a versatile substrate to manufacture composites with extensive nanomaterials. The energy storage performance of these three nanocomposites have been further evaluated with chronopotentiometry, and the corresponding curves are given in Figure 3c, 3e, & 3g. Different from that of graphene electrodes, the shapes of all curves are distorted, no longer triangular shape, due to the redox reactions at a certain potential, which will finally lead to a potential-dependent capacitance. Although their shapes are still not the same as that of battery-type electrodes, coulomb should be a better unit to evaluate their performance, instead of farad [25]. One can see, at any current densities, much longer charge/discharge time can be obtained for the prepared composites than that of the G-240, which means the much more charges can be stored

inside (Figure 3h&3i). The maximal capacity increases to ca. 22 times from 24.5 mC cm^{-2} for G-240 to 565.5 mC cm^{-2} for PANI-G at the current density of 0.5 mA cm^{-2}. For sure, different composites show different energy storage behaviors, and better performance could be achieved with further optimizations. All samples show more than 85% capacity retention after 1,000 consecutive cycles at a scan rate of 100 mV s^{-1} (Figure S10). The impedance data of MnO_2 and PANI samples before and after long-term cycling have been enriched in Figure S11. Their spectra are composed a semicircle and long tail, indicative of a charge transfer and a capacitor-like behavior. Besides, there is no obvious change between pristine sample and that after cycling, which indicates their stable structure. Concerning the impedance of Fc-MS functionalized sample, one can refer to our previous work [26,27].

The energy storage of the three composites involves charge transfer processes across the electrode interfaces, which is much more complicated than the pristine G-240 material. Therefore, the identification of the rate-determining step should be meaningful to improve their energy storage characteristics. The CV curves of the composites can maintain their originally intrinsic shapes only in a relatively slow scan rate range from mV s^{-1} to 20 mV s^{-1} (Figure 4a, 4d, and 4g). As the nature of the R-C circuit, serious polarization and the resistance-controlled behavior will occur in "high scan rates", which is due to the increased surface-capacitance as well as the resistance from the solution, electrode materials, and charge transfer processes. The definition of "high scan rates" is however different for different samples (Figure S12). As shown, obvious distortion occur at a scan rate of 50 mV s^{-1} for the PANI sample, but Fc-MS sample can still maintain its original shape at the scan rate of 200 mV s^{-1}, which means the Fc-MS could be used for power-type energy storage devices, as discussed in our previous work in detail, yet for non-flexible electrodes [26,27]. The rate-determining step of energy storage process in the low scan rates domain has also been analyzed by fitting the CV curves with the following equation (1):

$$i\,(V) = k_1 v + k_2 v^{0.5} \quad (1)$$

where $k_1 v$ and $k_2 v^{0.5}$ represent the surface-controlled current and diffusion-controlled current respectively. The fitting results (Figure 4b, 4e, and 4h) reveal that 57%, 77%, and 90% of total current come from the surface-controlled current at the scan rate of 10 mV s^{-1} for PANI, MnO_2, and Fc-MS respectively. This means that the ions diffusion resistances are also different during the energy storage process, and that the non-existing solid-state ions diffusion for the Fc-MS sample gives a much higher surface-controlled current ratio, even similar to that of G-240 electrode at 95 % (Figure S13). Similar trends can also be seen from fitting the redox peak currents vs. potential scan rates with the equation (2):

$$i = a v^b \quad (2)$$

where the empirical b value is an indicator of the type of reaction, ranging from 0.5 to 1 (0.5 for a diffusion-controlled behavior, and 1 for a surface-controlled charge transfer). The largest b value of Fc-MS (~0.91) demonstrates again a major surface-controlled redox process, in contrast to the diffusion-controlled behavior of PANI sample (b value of ~0.58).

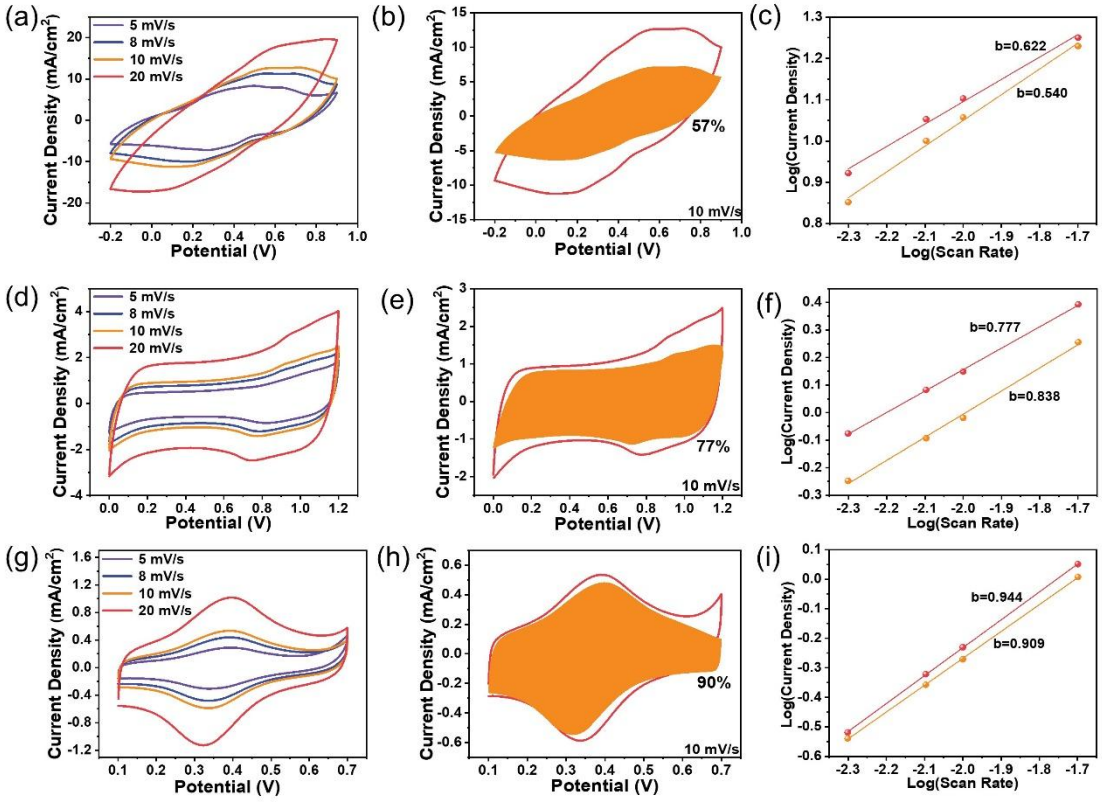

Figure 4. (**a**-**i**) The kinetic analysis of the energy storage behaviors of Fc-MS, MnO_2, and PANI: (**a**,**d**,**g**) the cyclic voltammetry of the three samples from 5 to 20 mV s^{-1}; (**b**,**e**,**h**) the calculated surface-controlled current from the respective CV curves (*vs.* Ag/AgCl 3 M); (**c**,**f**,**i**) the respective fitting slopes of the peak currents at different scan rates on a logarithmic scale.

2.4. Evaluation of a symmetrical device

Two pieces of PANI functionalized graphene electrodes have also been assembled into a symmetrical device to evaluate the possible practical application of the flexible graphene-based nanocomposite electrodes (Figure 5a-5d). The same acidic electrolyte as that above in a three-electrode configuration has been adopted to run the test for the assembled device. Figure 5a shows a group of CV curves from a scan rate of 5 mV s^{-1} to 200 mV s^{-1} in a potential window from -0.2 V to 0.9 V. A pair of broad redox peaks appear at ca. 0.3 V at the scan rate of 5 mV s^{-1}, which is consistent with that observed with the three-electrode system (Figure 4g), although being characterized by somewhat larger anodic-to-cathodic peak-to-peak separation. Indeed, the peak-polarization caused by the resistance is observed, especially with fastening the scan rate, but the rather symmetrical curves are still noticeable, even at the high scan rate of 200 mV s^{-1}, indicative of an expected rate performance. The areal capacitance of the device is examined by chronopotentiometry with applying various current densities ranging from 0.5 mA cm^{-2} to 4 mA cm^{-2} in a same potential window as CV tests, as plotted in Figure 5b. There is no obvious plateau, despite a little distortion, even at a small current density of mA cm^{-2}, which demonstrates the pseudocapacitive nature of the device. Its derived capacitances are given in Figure 5c, and one can see a high areal capacitance of 79.8 mF cm^{-2} at a current density of 0.5 mA cm^{-2}, and a 51.3% capacity retention at a current density of 4 mA cm^{-2}. Its Ragone plot is given in Figure 5d for its easy comparison with other similar film-type devices [28-32]. The present one can deliver a robust cycling performance, reaching a capacity retention of 78% after 1,000 consecutive cycles at a scan rate of 100 mV s^{-1} (Figure S14). Following this conceptual demonstration, future works could be di-

rected to replacing this 'classically' deposited PANI by PANI nanowire arrays exhibiting ultra-fast electrochemical responses [33].

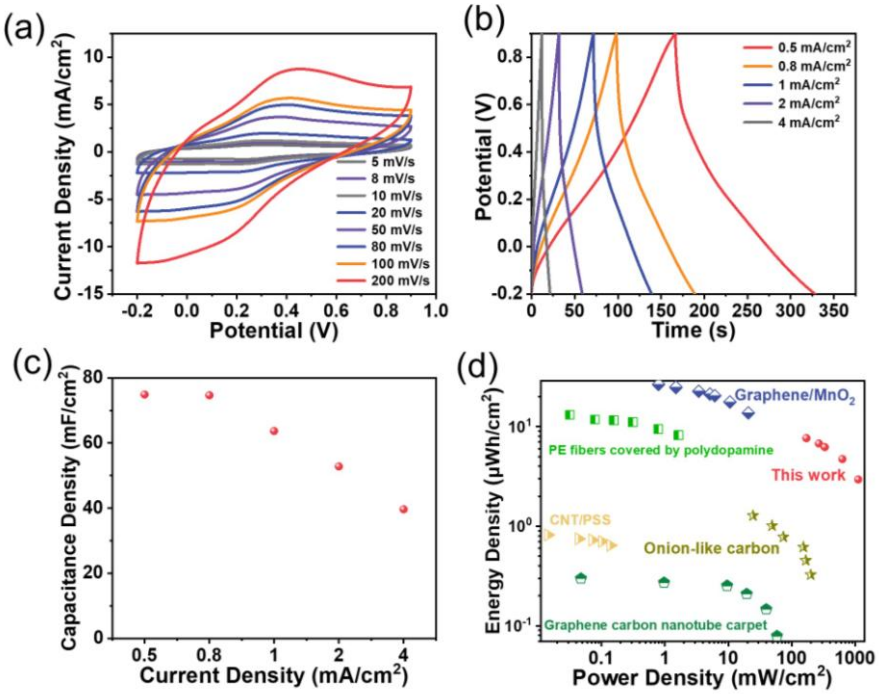

Figure 5. The energy storage performance of the PANI planar device in a symmetrical configuration: (**a**) the CV curves recorded at scan rates ranging from 5 to 200 mV s^{-1} in the potential window extending from -0.2 V to +0.9V; (**b**) the charge-discharge curves at current densities from 0.5 to 4 mA cm^{-2}; (**c**) the corresponding capacitance calculated from the charge-discharge curves; (**d**) the Ragone plot of this device and some reported benchmark devices: Graphene carbon nanotube carpet [28]; CNT/PSS [29]; Onion-like carbon [30]; PE fibers covered by polydopamine [31]; Graphene/MnO_2 [32].

3. Materials and Methods

Reagents. Tetraethoxysilane (TEOS, 98%), 3-chloropropyltrimethoxysilane (Cl-PTES, 97%), and graphite were purchased from Alfa Aesar, and cetyltrimethylammonium bromide (CTAB, 99%) was purchased from Acros. Acetonitrile (ACN, 99%), dimethylformamide (DMF, 99%), and cyclohexane (99%) were obtained from Merck. Ethynylferrocene (97%), lithium perchlorate (95%), lithium chloride (95%), copper sulfate (99%), sodium diethyldithiocarbamate trihydrate, and HCl (37%) were purchased from Sigma-Aldrich. Sodium nitrate (99%), ascorbic acid (97%), tetrabutylammonium bromide (99%), and poly(vinyl alcohol) (PVA, MW = 72,000 g/mol) originated from Fluka. Graphite foils and scotch tape were purchased from Shanghai Carbon Co. Ltd, and 3M, respectively. Sodium sulfate anhydrous (99%), manganese sulfate (95%), concentrated sulfuric acid (98%,) and aniline (99%) are from Meryer, Kaitong, Kermal, and Macklin, respectively. All compounds were used directly without further purification. The (3-azidopropyl) triethoxysilane (AzPTES) was synthesized with the protocol reported previously [34].

Apparatus. Transmission electron microscopy (TEM) investigation was performed with a JEOL ARM 200F – Cold FEG TEM/STEM equipped with a GIF Quantum ER. Scanning electron microscopy (SEM) analyses were carried out with a JEOL JSM-840 or Zeiss SUPRA 55 apparatus equipped with an energy-dispersive X-ray (EDX) microanalyzer and the high-resolution SEM micrographs have been obtained with the model JSM-IT500HR apparatus (JEOL). Atomic force microscopy (AFM) analysis was done with Asylum JEOL JSPM-5200. Raman spectroscopy measurements were carried out with a RenishawinVia spectrometer with a green light laser (532 nm). X-ray diffrac-

tion (XRD) pattern was obtained using the Nanoviewer from Rigaku (CuK α radiation) at a scanning rate of 5°/min.

Electrochemistry. Electrochemical experiments (including exfoliation of the graphite foil, electrodeposition of the silica film, PANI, MnO_2, cyclic voltammetry, and charge-discharge measurements) were performed with Autolab PGSTAT-300, μAutolab, or Biologic SP-150 potentiostat. The Ag/AgCl (3.5 M KCl) electrode and platinum plate (1 cm×1 cm) served as the reference electrode and counter electrode, respectively. An aqueous solution containing 1 M H_2SO_4 was used as the electrolyte for the performance test of the graphene samples, and PANI/Fc-MS functionalized samples, while 1 M Na_2SO_4 electrolyte was used for investigating the MnO_2 functionalized sample.

Preparation of the scotch tape-supported graphene samples (G-X, where X represents the exfoliation time). The laser cutting technique was first used to pattern the scotch tape to a certain design. Subsequently, the as-patterned scotch tape was pasted on the surface graphite foil followed by a peeling-off process to hand over a piece of graphite on the scotch tape. After that, similar to the electro-exfoliation method reported elsewhere [17], the electro-exfoliation process was further performed in 0.1 M Na_2SO_4 aqueous solution with a two-electrode system, where a piece of graphite coated scotch tape (graphite/scotch electrode) and platinum mesh (2.5 cm × 2.5 cm) were used as the working and counter electrode, respectively. The exfoliation was achieved by applying a voltage of 4 V for 240 s with a distance of 5 cm between the two electrodes. The obtained intermediate is highly resistive. To recover its conductivity, an activation process has been used via applying 0 V on the intermediate for 240 s in a three-electrode system with Ag/AgCl as the reference to remove the inserted sulfate ions. Finally, the as-prepared electrode, labeled as G-240, was thoroughly washed with deionized water and dried at room temperature overnight. Besides, different exfoliation times of 30 s, 120 s, and 360 s were also conducted to investigate the structural evolution, and the corresponding products were labeled as G-30, G-60, G-120, and G-360, respectively.

Preparation of the graphene-supported ferrocene functionalized silica thin film electrode (Fc-MS-G). The preparation protocol is similar to what we reported before [26], except a piece of G-240 was used as the working electrode in the present study. The finally obtained composite is labelled as Fc-MS-G for simplicity.

Preparation of the graphene-supported MnO_2 electrode (MnO_2-G). Cyclic voltammetry was used to deposit MnO_2 on the graphene surface with a three-electrode configuration, including a piece of G-240 as the working electrode, a platinum plate counter electrode, and Ag/AgCl (3 M) as reference electrode. The deposition was carried out within a potential window ranging from 0 V to +1.2 V at a scan rate of 10 mV s^{-1} in 0.1 M $MnSO_4$. After 40 consecutive cycles and thorough cleaning with water, one can obtain the MnO_2/graphene composite, labelled as MnO_2-G for simplicity.

Preparation of the graphene-supported PANI electrode (PANI-G). The same configuration of the MnO_2 preparation, but with a different electrolyte solution consisting of a mixture of 0.1 M H_2SO_4 and 0.01 M aniline, was used to prepare the graphene-supported PANI sample. The deposition process was achieved via 40 consecutive cycles in a potential window extending from -0.2 V to +1.0 V at a scan rate of 10 mV s^{-1}. After thoroughly cleaning with water, one can obtain the PANI/graphene composite, labelled as PANI-G for simplicity.

4. Conclusions

In this work, a laser-cutting coupled with electro-exfoliation protocol has been proposed to prepare planar graphene-based energy storage electrodes with a resolution of 800 μm. Compared to the graphene electrodes reported elsewhere, the electrodes prepared with this "Top-down" method well solve the tension between high conductivity and easy processability. The optimized G-240 graphene sample shows the rate performance of 40.8 mF cm^{-2} at a current density of 0.5 mA cm^{-2} and 81% (33.0 mF cm^{-2}) retention at a high current density of 8 mA cm^{-2}. The capacity can be further improved via

the formation of composites with other redox-active components, e.g., Fc-MS, MnO_2, and PANI in this work. The maximum capacity can increase 22 times to 565.5 mC cm^{-2} for the PANI functionalized sample, for instance. Thanks to the flexibility of the scotch tape substrate, a flexible symmetric pseudo-capacitor with a pair of PANI functionalized graphene electrodes has been assembled, showing a capacitance of 79.8 mF cm^{-2}. Such satisfactory results prove the protocol of this work in offering a new idea for the construction of flexible planar energy storage devices.

Supplementary Materials: The following supporting information can be downloaded at: www.mdpi.com/xxx/s1, Figure S1: (a) a typical exfoliation current for a piece of graphite foil; (b) Respective photographs of the final solution that exfoliates graphite-scotch tape and a piece of graphite under a same condition; Figure S2: the activation current profile of the G-240 at the potential of 0V for 240s; Figure S3: the XRD pattern of the set of graphite samples exfoliated at various times; Figure S4: the cross-section SEM view of the original graphite/scotch tape electrode; Figure S5: the TEM image of the G-240; Figure S6: the CV curve of the G-240 at a scan rate of 1 mV s^{-1} in 1M H_2SO_4 with a reference of Ag/AgCl (3 M); Figure S7: the cycling performance of G-240 at a scan rate of 100 mV s^{-1}; Figure S8: the impedance spectra of G-240 and G-240 after long-term cycling at OCP in the frequency range from 100 kHz to 0.1 Hz; Figure S9: the corresponding elements mapping results of (a) MnO_2, (b) PANI, and (c) Fc-MS functionalized samples to show their homogeneous distribution; Figure S10: the cycling performance of Fc-MS, MnO_2, and PANI at a scan rate of 100 mV s^{-1}; Figure S11: the impedance spectra of MnO_2 (a) and PANI (b) before and after long-term cycling at OCP in the frequency range from 100 kHz to 0.1 Hz; Figure S12: the CV curves of Fc-MS (a), MnO_2 (b), and PANI (c) at scan rates ranging from 20 mV s^{-1} to 200 mV s^{-1}; Figure S13: the surface-controlled current ratio of G-240 at a scan rate of 10 mV s^{-1}; Figure S14: the cycling performance of the PANI symmetrical device; Table S1 the impedance fitting parameters of the graphite, G-240, and G-240 before activation.

Author Contributions: "Conceptualization, J.W., N.V and A.W.; methodology, J.W. and N.V.; validation, J.W., N.V and A.W.; formal analysis, J.W.; investigation, J.W. and T.Y.; resources, A.W.; writing—original draft preparation, J.W.; writing—review and editing, N.V. and A.W.; visualization, J.W. and A.W.; supervision, N.V. and A.W.; project administration, J.W., N.V and A.W.; funding acquisition, J.W. and A.W. All authors have read and agreed to the published version of the manuscript.

Funding: This work was partly supported by the CNRS and the University of Lorraine. It also benefited from the financial supports of the National Natural Science Foundation of China (No.22105164) and the National Natural Science Foundation of Hebei Province (B2022203009).

Acknowledgment: J.W. acknowledges for the China Scholarship Council (CSC) for his doctoral studies.

Conflicts of Interest: The authors declare that they have no known competing financial interests or personal relationships that could have appeared to influence the work reported in this paper.

References

1. Kyerematen, N.A.; Brousse, T.; Pech, D. Microsupercapacitors as Miniaturized Energy-Storage Components for on-Chip Electronics. *Nat. Nanotechnol.* **2017**, *12*, 7–15, doi:10.1038/nnano.2016.196.
2. He, H.; Fu, Y.; Zhao, T.; Gao, X.; Xing, L.; Zhang, Y.; Xue, X. All-Solid-State Flexible Self-Charging Power Cell Basing on Piezo-Electrolyte for Harvesting/Storing Body-Motion Energy and Powering Wearable Electronics. *Nano Energy* **2017**, *39*, 590–600, doi:10.1016/j.nanoen.2017.07.033.
3. Dubal, D.P.; Chodankar, N.R.; Kim, D.H.; Gomez-Romero, P. Towards Flexible Solid-State Supercapacitors for Smart and Wearable Electronics. *Chem. Soc. Rev.* **2018**, *47*, 2065–2129, doi:10.1039/c7cs00505a.
4. Zhao, C.; Liu, Y.; Beirne, S.; Razal, J.; Chen, J. Recent Development of Fabricating Flexible Micro-Supercapacitors for Wearable Devices. *Adv. Mater. Technol.* **2018**, *3*, 1–16, doi:10.1002/admt.201800028.

5. Shao, Y.; Li, J.; Li, Y.; Wang, H.; Zhang, Q.; Kaner, R.B. Flexible Quasi-Solid-State Planar Micro-Supercapacitor Based on Cellular Graphene Films. *Mater. Horizons* **2017**, *4*, 1145–1150, doi:10.1039/c7mh00441a.
6. Zhang, C. (John); Nicolosi, V. Graphene and MXene-Based Transparent Conductive Electrodes and Supercapacitors. *Energy Storage Mater.* **2018**, *222*, 11–20, doi:10.1016/j.ensm.2018.05.003.
7. Kang, S.H.; Kim, I.G.; Kim, B.N.; Sul, J.H.; Kim, Y.S.; You, I.K. Facile Fabrication of Flexible In-Plane Graphene Micro-Supercapacitor via Flash Reduction. *ETRI J.* **2018**, *40*, 275–282, doi:10.4218/etrij.2017-0242.
8. Lamberti, A.; Clerici, F.; Fontana, M.; Scaltrito, L. A Highly Stretchable Supercapacitor Using Laser-Induced Graphene Electrodes onto Elastomeric Substrate. *Adv. Energy Mater.* **2016**, *6*, doi:10.1002/aenm.201600050.
9. Pu, X.; Liu, M.; Li, L.; Han, S.; Li, X.; Jiang, C.; Du, C.; Luo, J.; Hu, W.; Wang, Z.L. Wearable Textile-Based In-Plane Microsupercapacitors. *Adv. Energy Mater.* **2016**, *6*, doi:10.1002/aenm.201601254.
10. Liang, J.; Mondal, A.K.; Wang, D.W.; Iacopi, F. Graphene-Based Planar Microsupercapacitors: Recent Advances and Future Challenges. *Adv. Mater. Technol.* **2019**, *4*, 1–38, doi:10.1002/admt.201800200.
11. Mohan, V.B.; Jayaraman, K.; Stamm, M.; Bhattacharyya, D. Physical and Chemical Mechanisms Affecting Electrical Conductivity in Reduced Graphene Oxide Films. *Thin Solid Films* **2016**, *616*, 172–182, doi:10.1016/j.tsf.2016.08.007.
12. Chen, Y.; Xu, B.; Xu, J.; Wen, J.; Hua, T.; Kan, C.W. Graphene-Based in-Planar Supercapacitors by a Novel Laser-Scribing, in-Situ Reduction and Transfer-Printed Method on Flexible Substrates. *J. Power Sources* **2019**, *420*, 82–87, doi:10.1016/j.jpowsour.2019.02.096.
13. Gao, W.; Singh, N.; Song, L.; Liu, Z.; Reddy, A.L.M.; Ci, L.; Vajtai, R.; Zhang, Q.; Wei, B.; Ajayan, P.M. Direct Laser Writing of Micro-Supercapacitors on Hydrated Graphite Oxide Films. *Nat. Nanotechnol.* **2011**, *6*, 496–500, doi:10.1038/nnano.2011.110.
14. Wu, Z.S.; Parvez, K.; Feng, X.; Müllen, K. Graphene-Based in-Plane Micro-Supercapacitors with High Power and Energy Densities. *Nat. Commun.* **2013**, *4*, doi:10.1038/ncomms3487.
15. Li, L.; Secor, E.B.; Chen, K.S.; Zhu, J.; Liu, X.; Gao, T.Z.; Seo, J.W.T.; Zhao, Y.; Hersam, M.C. High-Performance Solid-State Supercapacitors and Microsupercapacitors Derived from Printable Graphene Inks. *Adv. Energy Mater.* **2016**, *6*, doi:10.1002/aenm.201600909.
16. Yang, Y.; Hou, H.; Zou, G.; Shi, W.; Shuai, H.; Li, J.; Ji, X. Electrochemical Exfoliation of Graphene-like Two-Dimensional Nanomaterials. *Nanoscale* **2019**, *11*, 16–33, doi:10.1039/c8nr08227h.
17. Parvez, K.; Wu, Z.; Li, R.; Liu, X.; Graf, R. Exfoliation of Graphite into Graphene in Aqueous Solutions. *J. Am. Chem. Soc.* **2014**, *136*, 6083–6091, doi:10.1021/ja5017156.
18. Munuera, J.M.; Paredes, J.I.; Enterría, M.; Pagán, A.; Villar-Rodil, S.; Pereira, M.F.R.; Martins, J.I.; Figueiredo, J.L.; Cenis, J.L.; Martínez-Alonso, A.; et al. Electrochemical Exfoliation of Graphite in Aqueous Sodium Halide Electrolytes toward Low Oxygen Content Graphene for Energy and Environmental Applications. *ACS Appl. Mater. Interfaces* **2017**, *9*, 24085–24099, doi:10.1021/acsami.7b04802.
19. Pei, S.; Wei, Q.; Huang, K.; Cheng, H.M.; Ren, W. Green Synthesis of Graphene Oxide by Seconds Timescale Water Electrolytic Oxidation. *Nat. Commun.* **2018**, *9*, 1–9, doi:10.1038/s41467-017-02479-z.
20. Khakpour, I.; Baboukani, A.R.; Forouzanfar, S.; Allagui, A.; Wang, C. In-Situ Exfoliation and Integration of Vertically Aligned Graphene for High-Frequency Response on-Chip Microsupercapacitors. *J. Power Sources* **2021**, *516*, 230701, doi:10.1016/j.jpowsour.2021.230701.
21. Parvez, K.; Li, R.; Puniredd, S.R.; Hernandez, Y.; Hinkel, F.; Wang, S.; Feng, X.; Müllen, K. Electrochemically Exfoliated Graphene as Solution-Processable, Highly Conductive Electrodes for Organic Electronics. *ACS Nano* **2013**, *7*, 3598–3606, doi:10.1021/nn400576v.

22. Sutto, T.E.; Duncan, T.T.; Wong, T.C. X-Ray Diffraction Studies of Electrochemical Graphite Intercalation Compounds of Ionic Liquids. *Electrochim. Acta* **2009**, *54*, 5648–5655, doi:10.1016/j.electacta.2009.05.026.
23. Pimenta, M.A.; Dresselhaus, G.; Dresselhaus, M.S.; Cançado, L.G.; Jorio, A.; Saito, R. Studying Disorder in Graphite-Based Systems by Raman Spectroscopy. *Phys. Chem. Chem. Phys.* **2007**, *9*, 1276–1290, doi:10.1039/B613962K.
24. Ferrari, A.C. Raman Spectroscopy of Graphene and Graphite: Disorder, Electron-Phonon Coupling, Doping and Nonadiabatic Effects. *Solid State Commun.* **2007**, *143*, 47–57, doi:10.1016/j.ssc.2007.03.052.
25. Yang, J.; Gunasekaran, S. Electrochemically Reduced Graphene Oxide Sheets for Use in High Performance Supercapacitors. *Carbon N. Y.* **2013**, *51*, 36–44, doi:10.1016/j.carbon.2012.08.003.
26. Wang, J.; Vilà, N.; Walcarius, A. Electroactive Organically Modified Mesoporous Silicates on Graphene Oxide-Graphite 3D Architectures Operating with Electron-Hopping for High Rate Energy Storage. *Electrochim. Acta* **2021**, *366*, 13407, doi:10.1016/j.electacta.2020.137407.
27. Wang, J.; Vilà, N.; Walcarius, A. Redox-Active Vertically Aligned Mesoporous Silica Thin Films as Transparent Surfaces for Energy Storage Applications. *ACS Appl. Mater. Interfaces* **2020**, *12*, 24262–24270, doi:10.1021/acsami.0c03650.
28. Lin, J.; Zhang, C.; Yan, Z.; Zhu, Y.; Peng, Z.; Hauge, R.H.; Natelson, D.; Tour, J.M. 3-Dimensional Graphene Carbon Nanotube Carpet-Based Microsupercapacitors With High Electrochemical Performance. *Nano Lett.* **2013**, *13*, 72–78, doi:10.1021/nl3034976.
29. Sim, H.J.; Choi, C.; Lee, D.Y.; Kim, H.; Yun, J.H.; Kim, J.M.; Kang, T.M.; Ovalle, R.; Baughman, R.H.; Kee, C.W.; et al. Biomolecule Based Fiber Supercapacitor for Implantable Device. *Nano Energy* **2018**, *47*, 385–392, doi:10.1016/j.nanoen.2018.03.011.
30. Pech, D.; Brunet, M.; Durou, H.; Huang, P.; Mochalin, V.; Gogotsi, Y.; Taberna, P.L.; Simon, P. Ultrahigh-Power Micrometre-Sized Supercapacitors Based on Onion-like Carbon. *Nat. Nanotechnol.* **2010**, *5*, 651–654, doi:10.1038/nnano.2010.162.
31. Du, J.; Wang, Z.; Yu, J.; Ullah, S.; Yang, B.; Li, C.; Zhao, N.; Fei, B.; Zhu, C.; Xu, J. Ultrahigh-Strength Ultrahigh Molecular Weight Polyethylene (UHMWPE)-Based Fiber Electrode for High Performance Flexible Supercapacitors. *Adv. Funct. Mater.* **2018**, *28*, 1707351–1707360, doi:10.1002/adfm.201707351.
32. El-Kady, M.F.; Ihns, M.; Li, M.; Hwang, J.Y.; Mousavi, M.F.; Chaney, L.; Lech, A.T.; Kaner, R.B. Engineering Three-Dimensional Hybrid Supercapacitors and Microsupercapacitors for High-Performance Integrated Energy Storage. *Proc. Natl. Acad. Sci. U. S. A.* **2015**, *112*, 4233–4238, doi:10.1073/pnas.1420398112.
33. Ullah, W.; Herzog, G.; Vilà, N.; Walcarius, A. Polyaniline Nanowire Arrays Generated Through Oriented Mesoporous Silica Films: Effect of Pore Size and Spectroelectrochemical Response. *Faraday Discuss.* **2022**, *233*, 77–99. doi:10.1039/D1FD00034A
34. Vilà, N.; Ghanbaja, J.; Aubert, E.; Walcarius, A. Electrochemically Assisted Generation of Highly Ordered Azide-Functionalized Mesoporous Silica for Oriented Hybrid Films. *Angew. Chemie - Int. Ed.* **2014**, *53*, 2945–2950, doi:10.1002/anie.201309447.